Crystal Structures of Human Mitochondrial Branched Chain Aminotransferase Reaction Intermediates: Ketimine and Pyridoxamine Phosphate Forms†

Neela H. Yennawar,*,‡ Myra E. Conway,§ Hemant P. Yennawar,‡ Gregory K. Farber,‡,|| and Susan M. Hutson§

Department of Biochemistry and Molecular Biology, Althouse Laboratory, The Pennsylvania State University, University Park, Pennsylvania 16802, and Department of Biochemistry, Wake Forest University School of Medicine, Winston-Salem, North Carolina 27157

Received March 20, 2002; Revised Manuscript Received June 13, 2002

ABSTRACT: The three-dimensional structures of the isoleucine ketimine and the pyridoxamine phosphate forms of human mitochondrial branched chain aminotransferase (hBCATm) have been determined crystallographically at 1.9 Å resolution. The hBCATm-catalyzed transamination can be described in molecular terms together with the earlier solved pyridoxal phosphate forms of the enzyme. The active site lysine, Lys202, undergoes large conformational changes, and the pyridine ring of the cofactor tilts by about 18° during catalysis. A major determinant of the enzyme's substrate and stereospecificity for L-branched chain amino acids is a group of hydrophobic residues that form three hydrophobic surfaces and lock the side chain in place. Short-chain aliphatic amino acid side chains are unable to interact through van der Waals contacts with any of the surfaces whereas bulky aromatic side chains would result in significant steric hindrance. As shown by modeling, and in agreement with previous biochemical data, glutamate but not aspartate can form hydrogen bond interactions. The carboxylate group of the bound isoleucine is on the same side as the phosphate group of the cofactor. These active site interactions are largely retained in a model of the human cytosolic branched chain aminotransferase (hBCATc), suggesting that residues in the second tier of interactions are likely to determine the specificity of hBCATc for the drug gabapentin. Finally, the structures reveal a unique role for cysteine residues in the mammalian BCAT. Cys315 and Cys318, which immediately follow a β-turn (residues 311−314) and are located just outside the active site, form an unusual thiol−thiolate hydrogen bond. This β-turn positions Thr313 for its interaction with the pyridoxal phosphate oxygens and substrate α-carboxylate group.

Branched chain amino acid aminotransferases (BCAT;[1] EC 2.6.1.42) are pyridoxal phosphate- (PLP-) dependent enzymes that catalyze reversible transamination of the L-branched chain amino acids to their respective α-keto acids. The BCAT enzymes are found in both bacteria and higher organisms (*1*−*3*). Bacteria have one BCAT enzyme (reviewed in ref *3*). Mammals have both a mitochondrial (BCATm) and a cytosolic (BCATc) form of the enzyme (*4*, *5*). Human BCATm (hBCATm) is the predominant form and is expressed ubiquitously in body tissues. In contrast, human BCATc (hBCATc) is found primarily in the central nervous system (*1*, *3*, *6*, *7*). These enzymes have important roles in body and brain nitrogen metabolism (*3*). The human isozymes are 58% identical in amino acid sequence and have similar substrate specificity (*8*−*10*). However, subtle differences in kinetic and physical properties of the two proteins, including inhibition of hBCATc but not hBCATm by the neuroactive drug gabapentin [1-(aminomethyl)cyclohexaneacetic acid], have been reported (*10*, *11*). The molecular basis for the specificity of gabapentin for hBCATc is not yet understood.

The mammalian BCATs are homodimers with molecular masses ranging from about 41000 to 46000. The molecular mass of the hBCATm subunit is 41300; each monomer consists of 365 amino acid residues and requires 1 pyridoxal phosphate (PLP) as cofactor (*10*, *12*). The *Escherichia coli* BCAT (eBCAT) enzyme and the related BCAT from *Salmonella typhimurium* are homohexamers with a subunit molecular mass of 31500. The crystal structure of the PLP form of eBCAT shows that it is an assembly of three dimer units around a 3-fold axis (*13*). In addition to differences in macromolecular structure and molecular mass, the human isozymes differ from these two bacterial BCATs in their sensitivity to sulfhydryl reagents and requirement for a reducing agent such as dithiothreitol (DTT) to preserve enzymatic activity. The *S. typhimurium* BCAT is not sensitive to sulfhydryl reagents such as the mammalian BCAT. Recent studies of hBCATm indicate that reversible oxidation of the two reactive cysteine residues, Cys315 and Cys318, by hydrogen peroxide to yield a disulfide bond results in complete inhibition of the enzyme. This CXXC motif therefore represents a potential redox-controlled switch on this enzyme (*14*).

† This work was supported by NIH Grant DK34738.

* To whom correspondence should be addressed. Tel: (814) 865-8383. Fax: (814) 863-7024. E-mail: nhy1@psu.edu.

‡ The Pennsylvania State University.

§ Wake Forest University School of Medicine.

|| Present address: National Institutes of Health, 6705 Rockledge Drive, Room 6152, Bethesda, MD 20892.

[1] Abbreviations: BCAT, branched chain aminotransferase; hBCATm, human mitochondrial branched chain aminotransferase; hBCATc, human cytosolic branched chain aminotransferase; eBCAT, *Escherichia coli* branched chain aminotransferase; PLP, pyridoxal phosphate; PMP, pyridoxamine phosphate; DAAT, D-amino acid aminotransferase; ADCL, 4-amino-4-deoxychorismate lyase; AspAT, aspartate aminotransferase; DTT, dithiothreitol; PEG, poly(ethylene glycol); RMSD, root mean square deviation.

10.1021/bi020221c CCC: $22.00
Published on Web 09/05/2002

PLP-dependent enzymes have been classified into four families with different fold types. Most aminotransferases, including the well-studied aspartate aminotransferases (AspAT) (*15*), belong to fold type I (*16*). The BCAT proteins, including those from eukaryotic and bacterial sources, are in the fold type IV family (*16*). Two other bacterial enzymes also belong to this family; D-alanine aminotransferase (DAAT) (*17*−*20*) catalyzes transamination of D-amino acids, whereas 4-amino-4-deoxychorismate lyase (ADCL) (*21*) converts 4-amino-4-chorismate to *p*-aminobenzoate and pyruvate. Unlike the fold type I enzymes, the fold type IV aminotransferases transfer the *pro-R* hydrogen (*17*). Available crystal structures (*12*, *13*, *18*, *19*, *21*, *22*) have confirmed the *re*-face specificity of this enzyme family.

The pathway for transamination proceeds by a ping-pong kinetic mechanism that consists of two half-reactions each with three main steps (*23*). In the PLP form, the cofactor is bound to the enzyme by an internal aldimine, with a Schiff base between an active site lysine and the PLP cofactor (*12*, *13*, *23*). Upon binding of a substrate amino acid, a transaldimination reaction occurs releasing the lysine residue, and an external aldimine between substrate and PLP is formed. The lysine is the catalytic base in the next step, a 1,3-prototropic shift that converts the external aldimine into a ketimine intermediate (*24*). In this step a proton is abstracted from the α-carbon of the substrate amino acid, and subsequent reprotonation of the aldehyde carbon of the coenzyme yields the ketimine. The final step in the first half-reaction is the hydrolysis of the ketimine to give the pyridoxamine phosphate (PMP) form of the enzyme and an α-keto acid. The second half-reaction is the reversal of the first half-reaction with a different keto acid.

The crystal structures of the PLP forms of eBCAT (*13*), hBCATm (*12*), and eBCAT with substrate analogues (*22*) have shed light into steps leading to formation of the external aldimine and residues involved in substrate binding. Herein we report two new structures, solved to 1.9 Å resolution, representative of several reaction intermediates, those of a branched chain amino acid substrate bound to the enzyme as a ketimine intermediate and of the enzyme with PMP and the α-keto acid product of the first half-reaction in the active site of one of the monomers. These and the earlier determined pyridoxal phosphate form (*12*) of the enzyme have enabled us to describe reaction pathway intermediates and amino acid substrate specificity of hBCATm in molecular terms.

MATERIALS AND METHODS

Expression of mature hBCATm (no mitochondrial targeting sequence) in *E. coli* and purification of the expressed enzyme have been reported (*10*, *14*). The recombinant protein contains four additional residues (GSHM) at the amino terminus. These residues were not well defined in the electron density map and are not included in the deposited hBCATm structures.

Crystallization, Soaking, and Data Collection. Yellow crystals of the PLP form (internal aldimine) of hBCATm were grown as described previously (*12*). Crystals that were chosen were in the orthorhombic form and exhibited the $P2_12_12_1$ space group symmetry with a dimer in the asymmetric unit.

Table 1: X-ray Data Collection and Refinement Statistics

data parameters	Val-soaked crystal	Ile-soaked crystal
space group	$P2_12_12_1$	$P2_12_12_1$
unit cell (Å)		
a	69.450	69.475
b	105.308	105.457
c	107.829	107.429
resolution range (Å)	20.0−1.9	19.7−1.9
integrated reflections	246448	238575
independent reflections	62273	61939
data completeness (highest shell) (%)	98.4 (91.1)	95.6 (90.3)
av I/av $\sigma(I)$ (highest shell)	21.5 (2.2)	17.4 (0.9)
R-merge (%) (highest shell)[a]	5.7 (40.3)	6.9 (66.6)
resolution limits (Å)	20.0−1.9	19.7−1.9
R-factor (working) (%)/no. of reflns	24.0/61024	24.3/60100
R-factor (free) (%)/no. of reflns	28.7/3077	28.4/3028
protein atoms	5820	5820
water molecules	244	221
cofactor atoms	32	48
acetates/glycerol	7/1	6/1
RMSD bond lengths (Å)	0.018	0.019
RMSD bond angles (deg)	2.0	2.2
average *B*-factors (Å)^2		
all atoms	36.5	37.2
protein main chain	35.6	36.5
protein side chain	37.3	37.9
external aldimine/PMP	32.4	36.9
waters/acetates/glycerol	42.1	42.8

[a] $R\text{-merge} = \Sigma|I_{obs} - \langle I_{obs}\rangle|/\Sigma\langle I_{obs}\rangle$.

To capture intermediates along the reaction pathway, the crystals were soaked in the crystallization solution with an excess amount of the substrates (*25*), either isoleucine or valine. The yellow crystals became colorless with time, indicating that the substrates had reacted beyond formation of the external Schiff base. The optimized soak conditions required substrate concentrations of 15 mM isoleucine or 25 mM valine and a gradual color change (2.5−3 h). The crystals were then transferred to a fresh crystallization solution containing the substrates and 10% glycerol (as a cryoprotectant) and frozen directly in the liquid nitrogen cold stream.

Diffraction data for the native, isoleucine-soaked, and valine-soaked crystals were collected at 100 K on beam line 5.0.2 of the Advanced Photon Source (Chicago, IL) with a 2 × 2 array CCD detector, using 1.071 Å wavelength radiation monochromatized with a double crystal Si(111). DENZO (*26*) and SCALEPACK were used to reduce the data. Crystal data are listed in Table 1.

Structure Determination. The molecular replacement method allowed for the solution of the substrate-soaked crystal structures using the earlier solved PLP forms of hBCATm as the search probe in the program AmoRe (*27*), which is part of CCP4 program suite (*28*). The program CNS (*29*) was then used for all further refinements. Torsion angle simulated annealing refinement was used to minimize model bias. The program O (*30*, *31*) was used for examination of electron density maps and manual adjustment of the model during refinement. Several cycles of positional refinement and isotropic *B*-factor refinement were performed after every model building cycle. The PLP was removed from the initial refinement cycles to get an unbiased view of the active site. Toward the end of the refinement, σ_A-weighted difference Fourier maps and $2F_o - F_c$ maps clearly showed the changes that had occurred at the active site because of the soaks. In

the isoleucine substrate soaked crystals, the active site density maps (Figure 1A,B) indicated that the substrate was bound as a ketimine in both monomers A and B. The isoleucine part of the ketimine refined well at an occupancy of 0.80 as judged from the density and the *B*-factors (Table 1).

In the valine-soaked crystal structure, we see a different intermediate. Here the active site density shows that the first half of the reaction has proceeded to completion, resulting in the PMP form (Figure 1C,D). There is also weak density indicating that the product from the first half-reaction, α-ketoisovalerate (Figure 1C), occupies the active site in one of the monomers. Its occupancy refined to 0.80 as judged from the *B*-factors and $2F_o - F_c$ density maps. The other monomer has two water molecules in the equivalent keto oxygen and carboxylate positions of the product (Figure 1D).

Water molecules were automatically located using CNS (*29*) and manually checked in O (*30*, *31*). In addition, acetate and glycerol molecules were modeled in manually into σ_A-weighted ($2F_o - F_c$) maps. A total of 221 and 244 water molecules, 6 and 7 acetate molecules, and 1 glycerol molecule each were located in the structures of crystals soaked with isoleucine and valine, respectively. Further model building and refinement cycles resulted in crystallographic *R*-factors, *R*-cryst and *R*-free of 0.243 and 0.284, respectively, for the crystals soaked with isoleucine and 0.24 and 0.287 for the crystals soaked with valine. The final model consists of 2 × 365 residues, 2 × PLP covalently linked to isoleucine in the ketimine form or 2 × PMP and an α-ketoisovalerate product in one of the monomers of the valine-soaked crystals and the bound acetate, glycerol, and water molecules. The average *B*-factors for these structures are given in Table 1.

Analysis of the stereochemistry of both of the structures with PROCHECK (*32*) showed that, in the isoleucine-soaked form, 86.5% and 11% of the main-chain atoms fall within the most favored region and additionally allowed regions of the Ramachandran plot, respectively. Ala172, Ile265, and Lys326 of the A monomer and Ser3, Ser4, and Ile53 of the B monomer are in the disallowed regions of the Ramachandran map. In the valine-soaked crystal 87% and 10.7% of the main-chain atoms fall within the most favored region and additionally allowed regions of the Ramachandran plot, respectively. Ala172, His233, and Lys326 of monomer A and Ser3 and Ser4 of monomer B are in the disallowed region of the Ramachandran map. There is clear density only at low contour levels for these residues. These residues are either part of the N-terminus or follow a residue with two possible side-chain conformations or are on surface loops and are distant from the active site. Part of the interdomain loop in monomer A, between residues 174 and 178 in the ketimine form, is disordered, and its electron density cannot be traced. Further, the density for residues 1−3 and 26 (monomer A) and 1−3, 23−27, 83, and 84 (monomer B) is connected only at low contours levels, indicating possible disorder. Residues 174−178 of monomer A are omitted from the ketimine model. In the PMP structure, residues 172−178 appear connected only at 0.8σ level contours in a $2F_o - F_c$ density map in monomer A, and density for residues 1−3, 26, and 27 of monomer B also appears connected only at lower contours. The coordinates for the isoleucine-soaked (1KT8) and valine-soaked (1KTA) hBCATm have been deposited in the Protein Data Bank.

RESULTS AND DISCUSSION

Overall Structure and Loop Movements. The PLP forms of hBCATm, the hBCATm inhibited with Tris (*12*), and the new structures reported in this paper all retain the overall fold of the other fold type IV proteins. The catalytically competent structure is a dimer; each monomer has two domains, and the active site is located at the domain interface (*10*, *12*). In the hBCATm monomer, the small domain (1−170) and the large domain (182−365) are connected by a flexible loop (residues 171−181). When the PLP forms of hBCATm were compared to the smaller eBCAT, there were differences in secondary structural elements (*12*). Out of the six fairly long helices, five are increased in length in hBCATm compared to eBCAT. There are 33 more residues at the N-terminus of mature hBCATm, which mostly lacks regular secondary structure and is flexible.

In the fold type IV enzymes that have been studied with substrate bound, there is no evidence for an interdomain movement that results in a conformational change to close the active site upon substrate binding (*20*, *22*). Instead, the bacterial eBCAT active site closes by movement of the interdomain loop (*22*). The monomers in the various structures of hBCATm (two crystal forms in the PLP form, the ketimine form, the PMP form, and the Tris-inhibited form) superpose quite well with an average root mean square deviation (RMSD) of 0.871 Å for the backbone atoms of the protein. As illustrated in Figure 2, in the PLP, ketimine, and PMP structures significant differences in conformation were found only in three loops and the N-terminus. The loops are located between residues 19−33 (loop 1), 82−87 (loop 2), and 171−181 (loop 3 or interdomain loop) and are not part of the dimer interface. Loop 3, with deviations of up to 7.1 Å, and loop 1 are quite flexible. The density for parts of loop 3 is broken for monomer A in the PLP and the ketimine forms. Loop 3 is well ordered in the Tris-inhibited structure (*12*) in both of the monomers and in monomer B of all the other forms. In the PLP form (molecules in red), the loops tend to extend into the protein. In the PMP (molecules in green) and the ketimine forms (molecules in cyan), the loops are more or less between the two extreme positions seen in the PLP and Tris-inhibited forms (not shown for clarity). The flexibility of these loops is illustrated further by variations in the two monomers of the same enzyme (Figures 3 and 4). Structural differences in the individual monomers may also reflect snapshots of each monomer at slightly different stages in the reaction pathway resulting from the soak experiments. For example, in the PMP form of hBCATm the α-keto acid of valine is still in the active site of monomer A but has clearly been released from monomer B (Figure 1C,D).

Ketimine Form of hBCATm. The active site density of the crystals that had been soaked with isoleucine could be modeled and refined as a ketimine intermediate (Figure 1A,B). Residues at the active site of monomer B and depictions of the hydrogen-bonding interactions in both monomers are shown in Figure 3. Conversion of the internal aldimine to the ketimine is accompanied by a movement of the C4A atom of the cofactor by about 1.5 Å. As predicted (*20*) and seen in the eBCAT external aldimine structure (*22*), the phosphate of the cofactor and the carboxylate of the substrate are on the same side of the active site. The side

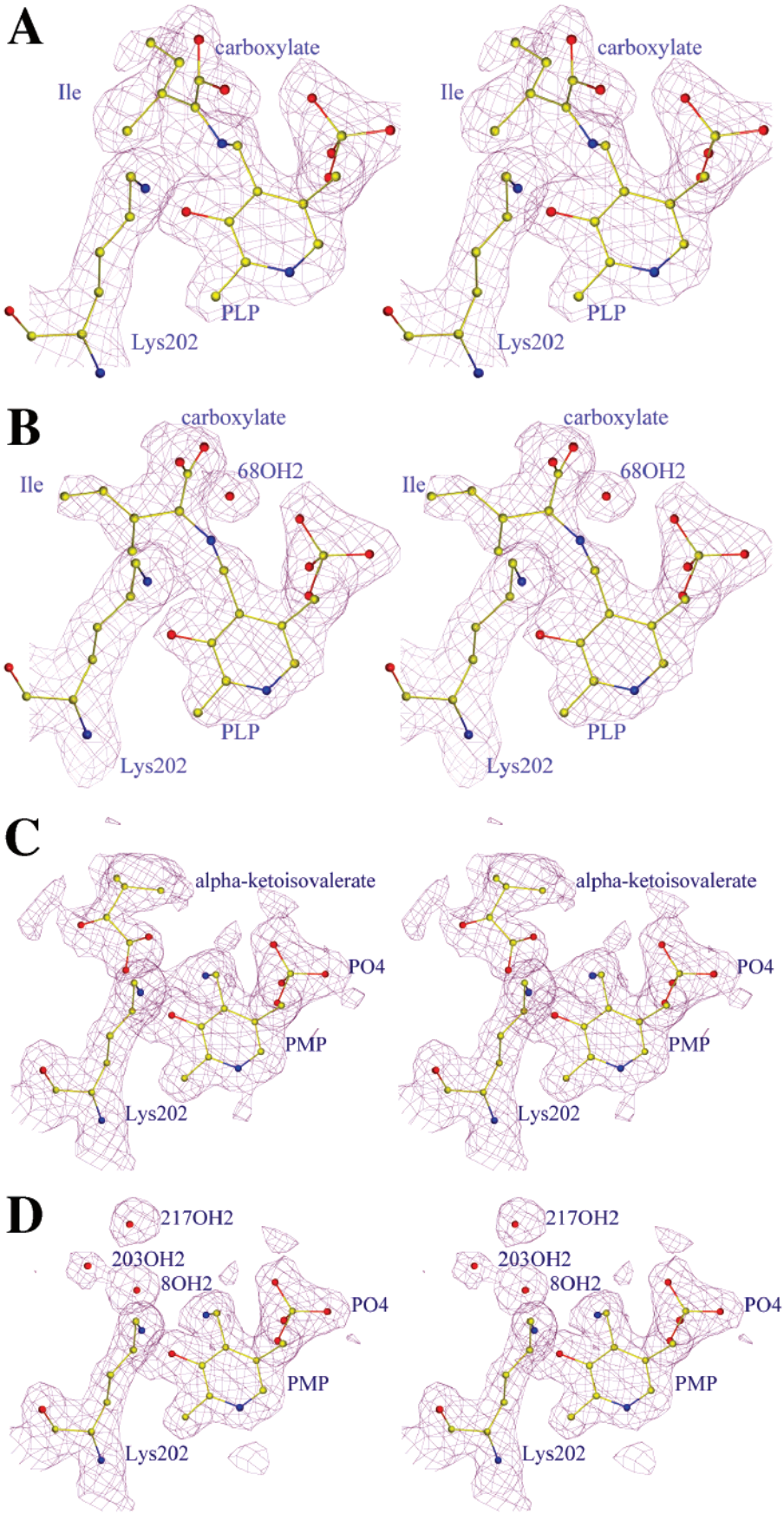

FIGURE 1: Stereoview of the $2F_o - F_c$ σ_A-weighted electron density in the region of the active site of the ketimine and PMP forms of hBCATm. Electron density is shown for monomer A (A) and monomer B (B) in the isoleucine-soaked crystal of hBCATm contoured at the 0.9σ level. The isoleucine substrate is covalently bound to the PLP at the N4A atom. Electron density is shown for monomer A (C) and monomer B (D) in the valine-soaked crystal of hBCATm. At low contour levels (0.7σ), the density for the product of the first half-reaction, α-ketoisovalerate, is seen in monomer A. The cofactor is in the PMP form.

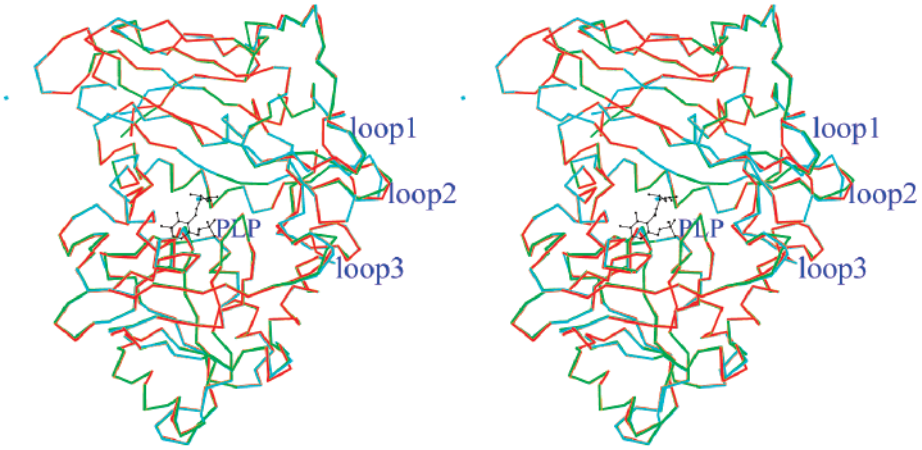

FIGURE 2: Superposition of the PLP, ketimine, and PMP forms of hBCATm monomer B. The program LSQKAB (*31*) was used. The PLP form is in red, the ketimine form in cyan, and the PMP form in green. Loop 1 (19−29), loop 2 (82−87), loop 3 (171−181), and the N-terminal residues show considerable variability. The average *B*-factors of the loops are 58.3, 52.7, and 57.8 Å^2, respectively.

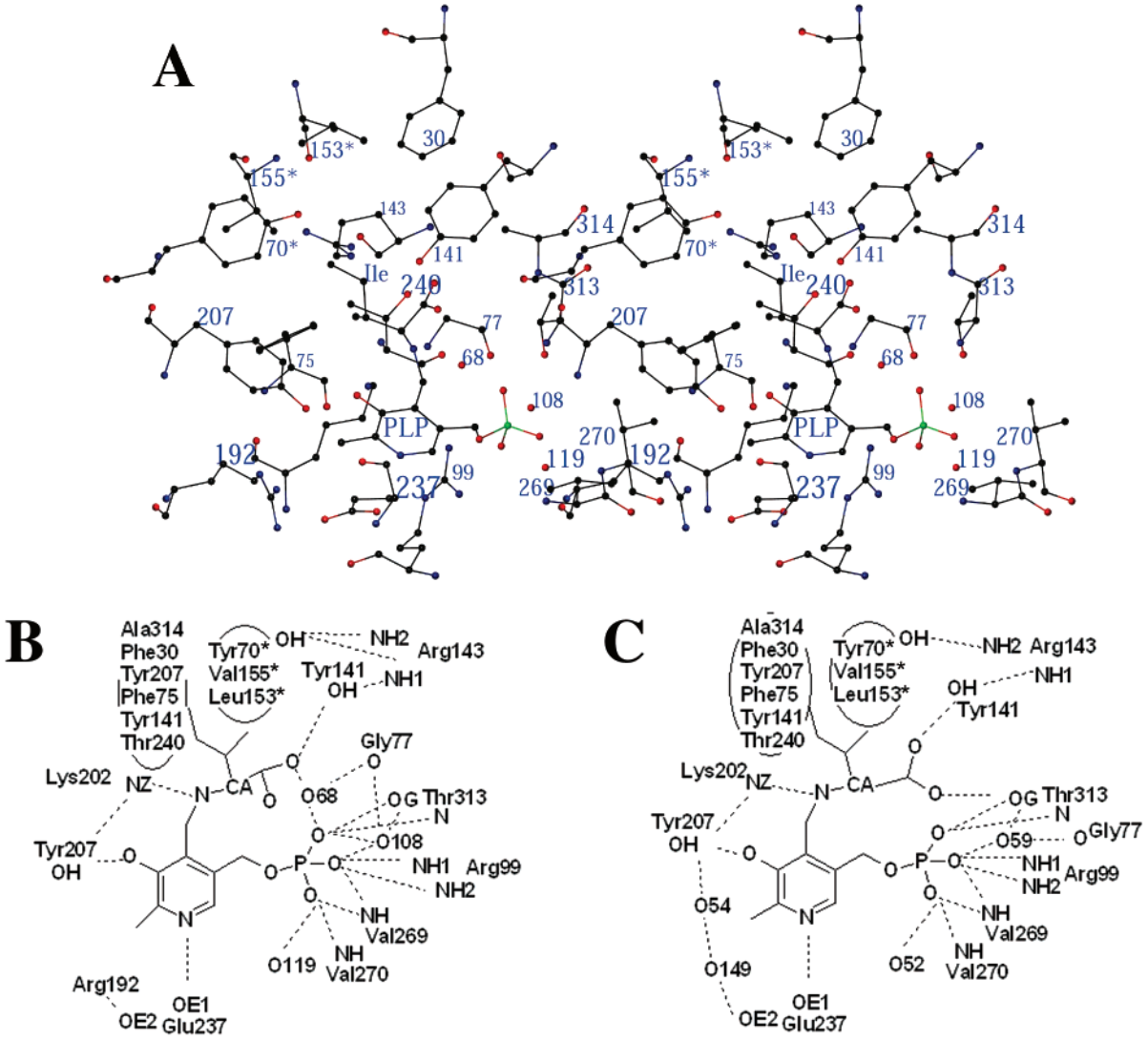

FIGURE 3: Stereoview of the active site in (A) monomer B of the ketimine form of hBCATm. The schematic diagram of the active site interactions (distances that are less than 3.4 Å) for monomers B and A are shown in (B) and (C), respectively, and were drawn using the program ISIS-Draw (MDL Information Systems, Inc., San Leandro, CA 94577). The PLP is located at the bottom of the active site pocket with its *re*-face toward the protein. The view is as seen down the *si*-face of the cofactor.

chains involved in binding the carboxylate (carboxylate binding pocket) are flexible. As shown in Figure 3A,B, in monomer B, the carboxylate of the substrate interacts with the hydroxyl of Tyr141 (2.40 Å) and also with the backbone oxygen of Gly77 through a water molecule (O68). The carboxylate in monomer B has moved just enough to allow

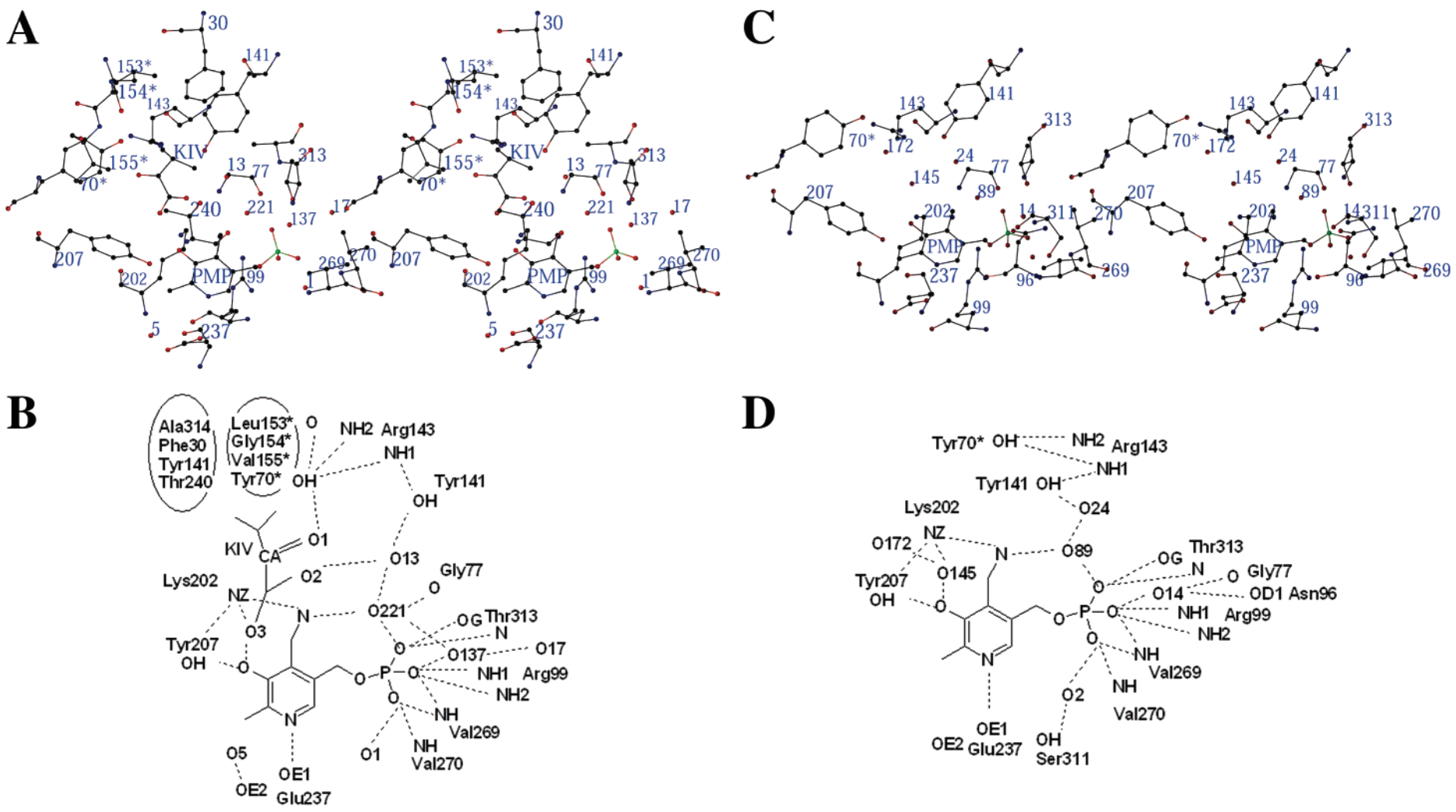

FIGURE 4: Stereoview of the active site in (A) monomer A and (C) monomer B of the PMP form of hBCATm. The orientation is the same as in Figure 3. The schematic diagram of the equivalent active site interactions (distances that are less than 3.4 Å) for monomers A and B are shown in (B) and (D). The product α-ketoisovalerate is still in the active site in monomer A.

a water molecule to insert itself between the carboxylate and the phosphate oxygens of the cofactor. In monomer A (Figure 3C), the carboxylate interacts with the side-chain hydroxyl of Thr313 (3.33 Å) and hydroxyl of Tyr141 (2.88 Å). Isoleucine displaces four water molecules, O45, O21, O46, and O100, that were observed in monomer A of the pyridoxal phosphate form (1EKF). In monomer B, isoleucine displaces two water molecules, O229 and O57.

The nonpolar residues Phe30, Tyr141, Tyr207, Phe75, Thr240, Ala314, Val155*, Tyr70*, and Leu153* surround and make van der Waals contacts with the nonpolar isoleucine side chain (Figure 3). These residues determine the way the substrate is oriented in the active site, rendering it suitable for the transamination reaction to proceed and the hydrogen to be abstracted from the Cα atom by the active site Lys202 NZ atom. Apart from these residues, there are other hydrophobic residues, Val29 (loop 1), Val170, Tyr173, and Phe174 (the latter two in interdomain loop 3), forming a substrate channel from the surface of the protein to the active site. There are also polar residues Lys32, Gln214, and Gln224 in this path that are folded into the protein matrix. Residues from both monomers form the active site and the substrate-binding pocket, thereby providing a structural basis for hBCATm to be active as a dimer (*10*). The interaction that completes the substrate-binding pocket and also helps to hold the dimer together is the hydrogen bonding of Tyr70* from monomer B with the guanidinium group of Arg143 from monomer A.

Comparison of the eBCAT structure with a substrate analogue bound as an external aldimine and the hBCATm ketimine structure shows the conservation of residues forming the substrate-binding pocket. Although the interdomain loops in eBCAT (residues 127−135) and hBCATm (residues 171−181) play a crucial role in both proteins, there are differences in the loops covering the active site pocket. The ordering of the interdomain loop observed on binding to substrate analogues in eBCAT (PDB codes 1I1M and 1I1L) results in a significant change in the side-chain conformation of Arg40. This redirection of the side chain of Arg40 is thought to trigger and stabilize the structural change to the closed form in eBCAT, whereas the interdomain loop covers the active site and shields the substrate from the solvent region (*22*). In contrast, in the hBCATm ketimine structure the interdomain loop has undergone significant conformation change (Figure 2). Lys79 of hBCATm occupies the equivalent position of Arg40 in eBCAT. This residue does not undergo any conformational change on substrate binding nor does it interact with the interdomain loop in any of the forms of hBCATm. However, in both monomers Tyr173, which is part of loop 3 and about 13 Å away from Lys202, moves on isoleucine (Cα atom shifts by 2.3 and 1.0 Å in monomers A and B, respectively) or valine binding (Cα atom shifts by 2.3 and 1.3 Å in monomers A and B, respectively) and consequently widens the access to the active site. The two monomers are opened up to different extents. In monomer A, a probable weak interaction is also formed between the sulfur at Cys315 and the π-electron cloud on Tyr173 (S−H$\cdot\cdot\cdot\pi$ hydrogen bond) (*34*) that presumably could stabilize the open conformation of the substrate-binding pocket in this monomer (*14*). This interaction is absent in monomer B although the ring atoms of Tyr173 approach S^{γ} of Cys315 (the closest distance between Tyr173 and Cys315 reduces from 3.9 Å in the PLP form to 3.2 Å in the ketimine form). The flexibility of loop 3 is also confirmed by the temperature factors. Thus, instead of domain closure as is classically seen in AspAT (*5*, *6*, *11*, *12*, *15*) or closure by movement of the interdomain loop as observed in eBCAT (*22*), in hBCATm, movement of the Tyr173 which is a part of the interdomain loop increases access to the active site. Residues 28−33 of loop 1 are close to the active site. In hBCATm, Phe30 forms part of the hydrophobic surface in the substrate-binding pocket. As stated above, loop 1 and the preceding residues are missing in the *E. coli* sequence.

PMP Form of hBCATm. The structure of hBCATm−PMP resulting from hBCATm crystals soaked with valine was refined at 1.9 Å resolution (Table 1 and Figure 1C,D). Residues at the active site and schematic diagrams of the hydrogen bond interactions are shown in Figure 4. There is weak density showing that the product of the valine half-reaction, α-ketoisovalerate, is bound in the active site substrate of monomer A (Figure 4A,B) whereas it has dissociated from monomer B (Figure 4C,D). Residues Leu153*, Gly154*, Val155*, Tyr70*, Tyr141, Phe30, Thr240, and Ala314 stabilize the α-ketoisovalerate (valine) side chain. Since the α-ketoisovalerate is not bound to the cofactor in monomer A, its α-carbon atom has moved by 4.7 Å with respect to the isoleucine ketimine intermediate. Nevertheless, most of the interactions with the side chain are similar to the isoleucine side chain of the ketimine intermediate. Exceptions are Tyr207 and Phe75, which interact with the isoleucine side chain in the ketimine structure but are not close enough to make van der Waals contact in the α-ketoisovalerate PMP intermediate, and Gly154*, which forms an interaction with the side chain of the product α-ketoisovalerate of the PMP intermediate but not to the isoleucine side chain in the ketimine intermediate (Figures 3A and 4A). The hydroxyl group on Tyr70* is at a hydrogen-bonding distance from the newly formed keto oxygen. The amino group of the PMP, NZ atoms of Lys202, the water molecule O13, and the oxygen on the pyridine ring all hydrogen bond with the carboxylate of the α-ketoisovalerate. These interactions may serve to direct the α-ketoisovalerate product out of the active site. In monomer B there are three water molecules, O145, O172, and O24, that have replaced the α-keto acid in the active site (Figure 4C,D). They occupy positions equivalent to the carboxylate oxygens and the α-keto oxygen of the product in monomer A.

The amino group of the pyridoxamine moiety forms hydrogen bond interactions with water molecules O221 in monomer A (2.89 Å) and O89 in monomer B (2.93 Å) and the NZ atom of the active site Lys202 (2.81 and 2.77 Å in monomers A and B). The latter atom participates in two more hydrogen bonds, one with the hydroxyl of Tyr207 (3.15 and 3.20 Å in monomers A and B) and the other with the carboxylate group of the α-ketoisovalerate product (3.13 Å) in monomer A and a water molecule (2.71 Å) in monomer B.

Active Site Lysine and PLP Cofactor in the hBCATm Structures. The flexible Lys202 side chain is seen in different conformations in each structure (Figure 5). This movement results in differences in the hydrogen bonding of the side chain in the different enzyme forms. In the internal aldimine, the lysine NZ donates a proton to the PLP phenolic oxygen, forming a hydrogen-bonding network with the hydroxyl of Tyr207, water O16, the main-chain carbonyl oxygen of

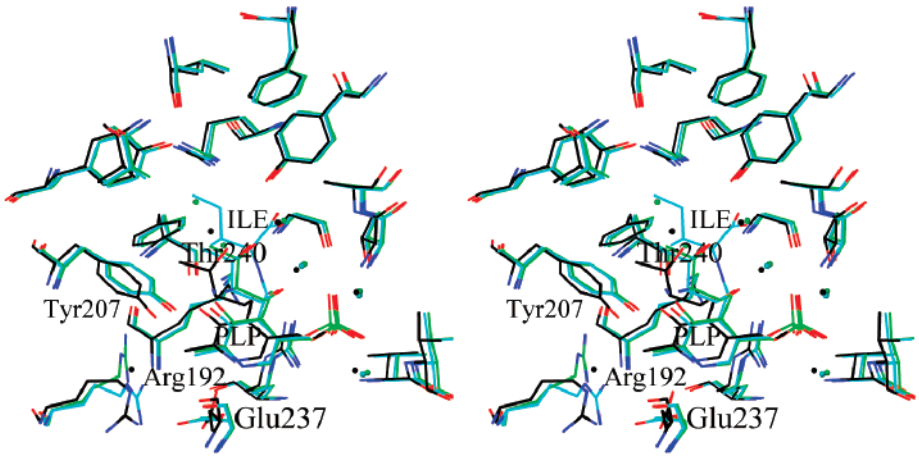

FIGURE 5: Superposition of the hBCATm active site residues for monomer B. The PLP form is in black, the isoleucine ketimine form is in cyan, and the PMP form is in green. The cofactor ring tilts by 18−19° away from the protein in the ketimine (except in monomer A), PMP, and the inhibitor forms compared to the PLP form. Tyr207 and Glu237, interacting with the pyridine ring of the PLP, rotate while retaining their hydrogen bonds. Thr240, which is in van der Waals contact with the ring on the *si*-side, moves as well. The flexible lysine (Lys202) undergoes large conformational changes. Arg192, interacting with Glu237, also undergoes a large side-chain reorientation.

Tyr201, and side chains of Asn206 and Arg192 (*12*). Tyr207 interacts with the phenolic oxygen of the cofactor in all of the hBCATm structures (Figures 3 and 4) (*12*). In the ketimine form, Lys202 NZ participates in two hydrogen bond interactions, one with the side-chain hydroxyl of Tyr207 and the other with the imine nitrogen of the ketimine (Figure 3B,C). In the PMP form of monomer A with α-ketoisovalerate in the active site (Figure 4A), Lys202 NZ atom forms a hydrogen-bonding network with Tyr207, the α-ketoisovalerate carboxylate O3, and the newly formed amino group of the pyridoxamine phosphate.

The cofactor is held in place in the active site of hBCATm by numerous noncovalent interactions, with the *si*-face of the pyridine ring toward the solvent and incoming substrates and the *re*-face toward the protein (Figures 3 and 4) (*12*). The strongest noncovalent interactions holding the cofactor to the protein involve interactions of the phosphate with the protein backbone and side-chain atoms. Many of the interactions made by the phosphate of the cofactor are identical in all four structures. The OP1 atom interacts with a water molecule, the hydroxyl, and the backbone nitrogen of Thr313. The OP2 atom interacts with the side chain of Arg99 and the backbone amide nitrogen of Val269. The OP3 atom interacts with a water molecule and the backbone amides of Val269 and Val270. The oxygen atoms on the phosphate are involved in 8−11 hydrogen bonds. The negative charge of the phosphate group is balanced by the positive charge of Arg99, the dipole of the α-helix (268−282) that has its N-terminus close to the phosphate group, and the aligned peptide dipoles of residues 312, 313, and 314 of the β-turn preceding Cys315 and Cys318. Glu237 forms an ion pair with the protonated N1 of the pyridine ring in all of the enzyme forms (Figure 5).

There are two important structural differences among the PLP, PMP, Tris-inhibited, and ketimine forms in the active site region: the rocking motion of the cofactor as it tilts about the axis defined by the phosphate group and the pyridine nitrogen and the conformation of Lys202. The PLP ring is tilted in the ketimine, Tris-inhibited, and the PMP structures by 18−19° compared to the PLP form, and the center of the ring moves on average by 0.29 Å (Figure 5). The tilt is away from Lys202. As the cofactor tilts, Tyr207 and Glu237 rotate to maintain their interactions with the pyridine ring nitrogen and oxygen of the PLP, respectively. As seen in Figure 5, Arg192, Glu237, Thr240, and Tyr207 reorient their side-chain conformations in the different forms, thus maintaining their respective interactions with the tilting ring of the cofactor.

Structural Role of Cys315 and Cys318. We have shown recently that labeling of Cys315 and Cys318 with sulfhydryl reagents or oxidation of the thiols to a disulfide bond results in the loss of hBCATm activity; these cysteine residues are, therefore, part of a redox-active CXXC center that regulates hBCATm activity (*14*). The cysteine sulfurs are located about 10 Å from the active site. Residues 312−314 preceding Cys315 form a β-turn whose peptide dipoles are involved in stabilizing the PLP phosphate (see above). Cys318 is at the beginning of the β-sheet structure. In all of the hBCATm crystal structures except that of the Tris-inhibited enzyme, Cys315 and Cys318 are in the reduced state with sulfur−sulfur distances ranging from 3.07 to 3.46 Å. This is substantially closer than the expected van der Waals radii (3.60 Å) (*35*) and is suggestive of a special interaction (*36*). Thiol−thiol hydrogen bonding is unlikely because that involves larger separations (*36*, *37*). In these structures (*12*), the average angles at Cβ−Sγ−Sγ for Cys315 and Cys318 are 119° and 68°, respectively, in monomer A, and 119° and 64°, respectively, in monomer B. The bond distances suggest that Cys315 and Cys318 form a thiol−thiolate hydrogen bond and the bond angles implicate Cys315 as the thiol and Cys318 as the attacking thiolate (*36*). This bond is not found in the Tris-inhibited structure of the enzyme (*12*) where the corresponding sulfur−sulfur bond distances are 4.20−4.30 Å. Consequently, the peptide dipole alignment and the hydrogen-bonding pattern seen at the β-turn (residues 311−314) in the PLP, PMP, and ketimine structures are disrupted in the Tris-inhibited structure (*14*). In the latter structure, Gln316 undergoes significant changes in its side-chain conformation and interacts with the backbone carbonyl oxygen at Thr313.

Mitochondrial AspAT and cytosolic AspAT also have a cysteine residue that is sensitive to sulfhydryl reagents (*38*,

39). However, this cysteine residue does not play a structural role. Rather, its location at the domain interface makes its environment susceptible to the structural change involved in the open to closed conformational transition. In hBCATm, the interaction between Cys315 and Cys318 may influence the backbone conformation of the protein at the β-turn between residues 311 and 314 and affect cofactor and substrate binding. Therefore, hBCATm is the first example of an aminotransferase where cysteine residues may play a structural role in catalysis (*14*).

Comparison with DAAT, ADCL, and eBCAT. In the other fold type IV enzymes, ADCL (*21*), DAAT (*20*), and eBCAT (*13*), the active site is comprised of residues from both domains of one monomer and the small domain of the other monomer. The *re*-face of the PLP ring faces the protein, and the catalytic lysine acts on the *re*-face of PLP. In the different forms of hBCATm the cofactor tilts by a maximum of 18−19° compared to about 30° in eBCAT and 25° in DAAT. Similar to the BCATs, ADCL and DAAT have an α-helix whose dipole stabilizes the charge on the phosphate. In DAAT, the carboxylate of the substrate is on the same side of the cofactor as the hydrophobic side-chain pocket in hBCATm. The cavity for the substrate side chain in DAAT is quite open, allowing the enzyme to accommodate a range of D-amino acids. The side-chain pocket in hBCATm is rather restricted, and that would account for the substrate specificity of this enzyme.

Substrate Specificity. The kinetic characterization of hBCATm (*10*) has shown that branched chain amino acids are the preferred substrates. Glutamate is also accepted, but not D-isoleucine, aspartate, aromatic amino acids, methionine, alanine, or glutamine. The ketimine structure shows that the side chain plays a crucial role in positioning the incoming substrate. Therefore, we modeled different substrate side chains into the substrate-binding pocket on the basis of the ketimine intermediate. The side-chain-binding pocket is determined by three surfaces. Surface A is on the same side as the amino group of the substrate and is formed by residues Phe75, Tyr207, and Thr240. Surface B is on the same side as the carboxyl group of the substrate and is formed by Phe30, Tyr141, and Ala314. Residues Tyr70*, Leu153*, and Val155* from the second monomer form surface C. The hydrogen bond interaction between Tyr70* and Arg143 is crucial for the closure of the active site by this surface.

The hydrophobic side chains of L-valine, L-isoleucine (Figure 6A), and L-leucine fit into the pocket bounded by A, B, and C and have van der Waals interactions with A and B. As seen in Figure 6B, an alanine side chain would fall short of interacting through van der Waals contacts with any of the surfaces. Bulky side chains such as those found in the aromatic amino acids (phenylalanine shown in Figure 6C) or the dicarboxylic acid amino acid aspartate (not shown) would have severe steric clashes with surfaces A and B in either of their minimum energy conformers. With the dicarboxylic amino acid substrate glutamate model (Figure 6D), the side-chain carboxylate forms good hydrogen bond interactions with the side chains of Tyr141 and Arg143 of monomer A and Tyr70* (surface C) of monomer B. Although glutamate and glutamine have side chains of the same length, only glutamate is accepted as a substrate.

Human BCAT is specific for L-amino acids, because modeling a D-enantiomer into the active site orients the carboxylate facing the hydrophobic surfaces A and B and the hydrophobic side chain facing the backbone carbonyl oxygen and amidic nitrogen of Gly77, the hydroxyls of Tyr141 and Thr313, or water molecules. L-*threo*-Isoleucine is preferred over L-*allo*-isoleucine (*10*). Unlike L-*threo*-isoleucine, the L-*allo*-isoleucine side-chain hydrophobic interactions are only geometrically possible with one (surface A or B) but not both of the surfaces. Also, the terminal methyl group would have to point toward the hydroxyl of Tyr141 or the guanidinium group of Arg143.

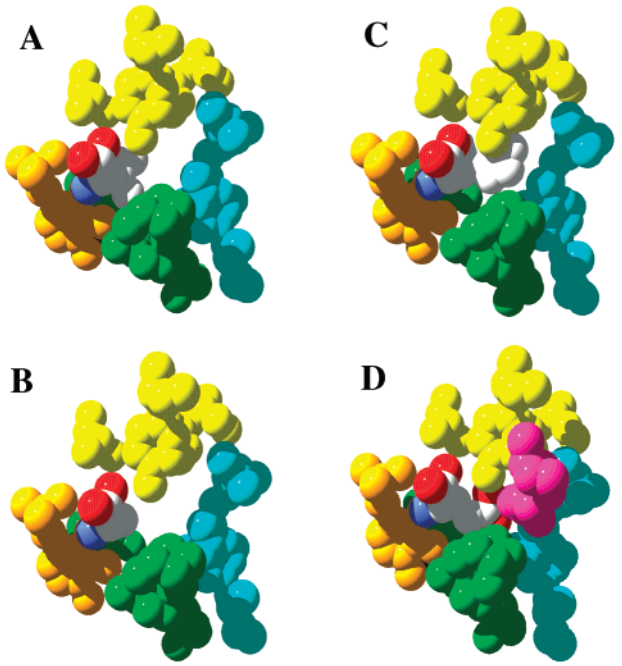

FIGURE 6: Space-filling diagrams of selected amino acids modeled into the hBCATm substrate side-chain-binding pocket. Three surfaces form this pocket. Phe75, Tyr207, and Thr240 form surface A (green). Surface B (yellow) comprises Phe30, Tyr141, and Ala314. Residues Tyr70*, Leu153*, and Val155* from the second subunit form surface C (cyan). The PLP cofactor is shown in orange. (A) In the ketimine structure, the isoleucine side chain forms van der Waals interactions with surfaces A and B. (B) L-Alanine, (C) L-phenylalanine, and (D) L-glutamate were modeling on the ketimine structure. The glutamate δ-carboxyl group shows favorable hydrogen bond interactions with Tyr141 (surface B) and Arg143 (in pink) of monomer A and Tyr70 (surface C) of monomer B.

Model of hBCATc. The cytosolic isozyme hBCATc is a target of the antiepileptic drug gabapentin (*11*). To date, there is no crystal structure available for hBCATc. On the basis of the backbone conformation structure of hBCATm, a model of hBCATc was built with the side chains accordingly mutated, the whole model energy was minimized using the SWISS-MODEL package (*40*), and the leucine analogue gabapentin was then modeled into the substrate-binding pocket with its carboxylate close to the carboxylate binding site of the isoleucine substrate and the cyclohexyl ring of the gabapentin in the branched chain binding pocket. The backbone of this model is essentially the same as hBCATm (RMSD = 0.67 Å). At the active site, all residues that would be interacting directly with the cofactor and possibly with gabapentin are conserved between hBCATm and hBCATc. In the next shell of interactions, i.e., those residues that are interacting with the residues that are interacting with the cofactor and gabapentin, 18 mutations might be indirectly affecting binding. Of these, the Ser156 to Lys change could

most affect substrate/gabapentin binding. Its position in the likely path leading to the active site (along with Tyr173) could provide steric hindrance for bound substrates/products/gabapentin to enter or leave the active site. Another mutation that could affect change in the binding is Val270 to Thr. This may stabilize the carboxylate of the incoming substrate by providing additional hydrogen-bonding species through its side-chain hydroxyl group.

Conclusions. As a result of soaking hBCATm crystals with substrate amino acids, we have been able to capture the enzyme and each monomer at several different stages of the reaction pathway. The structures provide a molecular explanation for the substrate specificity of hBCATm and show that, on substrate binding, hBCATm does not undergo the classic domain closure seen in AspAT (*15*) or the loop closure observed with eBCAT (*22*). Cysteine residues (Cys315 and Cys318) in hBCATm play a structural role. They form a thiol−thiolate hydrogen bond that may be crucial to the backbone geometry and hydrogen-bonding pattern around Thr313 (involved in cofactor and substrate stabilization). Finally, there is new evidence that alternatively spliced forms of hBCATm are expressed in human tissues and at least one of these proteins has a function that appears distinct from that of hBCATm (*41*, *42*). Structurally important residues are missing in both alternatively spliced forms of hBCATm. One protein lacks the mitochondrial targeting sequence (*42*), is missing Phe30 (surface A) and Tyr70* (surface C) of the side-chain-binding pocket, but still has the redox-active CXXC motif. Preliminary results suggest that this protein may not have BCAT activity. A second form has a 12 amino acid deletion (*41*) that starts immediately after Cys315. This deletion should affect the geometry of the turn at Cys315 and indirectly the geometry and hydrogen bonding at the β-turn involving Thr313. It has been reported that this protein is a co-repressor for a thyroid hormone nuclear receptor (*41*). Thus, hBCATm may join the growing list of metabolic enzymes that have functions that are independent of their enzymatic activity in a metabolic pathway.

ACKNOWLEDGMENT

The authors thank Dr. Leslie Poole and Dr. Conn Mallett for many helpful discussions and for critical reading of the manuscript. Use of the Advanced Photon Source was supported by the U.S. Department of Energy, Basic Energy Sciences, Office of Energy Research, under Contract W-31-109-ENG-38. Thanks are also due to Dr. Andrew Howard at the APS.

REFERENCES

1. Ichihara, A. (1985) *Aminotransferases of branched chain amino acids in transaminases* (Christen, P., and Metzler, D. E., Eds.) Vol. 2, pp 430−439, Wiley and Sons, New York.
2. Conway, M. E., and Hutson, S. M. (2000) *Methods Enzymol. 324*, 355−365.
3. Hutson, S. M. (2001) *Prog. Nucleic Acid Res. Mol. Biol. 70*, 175−206.
4. Hutson, S. M. (1988) *J. Nutr. 118*, 1475−1481.
5. Hutson, S. M., Fenstermacher, D., and Mahar, C. (1988) *J. Biol. Chem. 263*, 3618−3625.
6. Hutson, S. M., Wallin, R., and Hall, T. R. (1992) *J. Biol. Chem. 267*, 15681−15686.
7. Hall, T. R., Wallin, R., Reinhart, G. D., and Hutson, S. M. (1993) *J. Biol. Chem. 268*, 3092−3098.
8. Hutson, S. M., Bledsoe, R. K., Hall, T. R., and Dawson, P. A. (1995) *J. Biol. Chem. 270*, 30344−30352.
9. Bledsoe, R. K., Dawson, P. A., and Hutson, S. M. (1997) *Biochim. Biophys. Acta 1339*, 9−13.
10. Davoodi, J., Drown, P. M., Bledsoe, R. K., Wallin, R., Reinhart, G. D., and Hutson, S. M. (1998) *J. Biol. Chem. 273*, 4982−4989.
11. Hutson, S. M., Berkich, D., Drown, P., Xu, B., Aschner, M., and LaNoue, F. (1998) *J. Neurochem. 71*, 863−874.
12. Yennawar, N., Dunbar, J., Conway, M., Hutson, S., and Farber, G. (2001) *Acta Crystallogr. D57*, 506−515.
13. Okada, K., Hirotsu, K., Sato, M., Hayashi, H., and Kagamiyama, H. (1997) *J. Biochem. 121*, 637−641.
14. Conway, M. E., Yennawar, N., Wallin, R., Poole, L. B., and Hutson, S. M. (2002) *Biochemistry* (in press).
15. Rhee, S., Silva, M. M., Hyde, C. C., Rogers, P. H., Metzler, C. M., Metzler, D. E., and Arnone, A. (1997) *J. Biol. Chem. 272*, 17293−17302.
16. Grishin, N. V., Phillips, M. A., and Goldsmith, E. J. (1995) *Protein Sci. 4*, 1291−1304.
17. Yoshimura, T., Nishimura, K., Ito, J., Esaki, N., Kagamiyama, H., Manning, J. M., and Soda, K. (1993) *J. Am. Chem. Soc. 115*, 3897−3900.
18. Sugio, S., Petsko, G. A., Manning, J. M., Soda, K., and Ringe, D. (1995) *Biochemistry 34*, 9661−9669.
19. Sugio, S., Kashima, A., Kishimoto, K., Peisach, D., Petsko, G. A., Ringe, D., Yoshimura, T., and Esaki, N. (1998) *Protein Eng. 11*, 613−619.
20. Peisach, D., Chipman, D. M., Van Ophem, P. W., Manning, J. M., and Ringe, D. (1998) *Biochemistry 37*, 4958−4967.
21. Nakai, T., Mizutani, H., Miyahara, I., Hirotsu, K., Takeda, S., Jhee, K. H., Yoshimura, T., and Esaki, N. (2000) *J. Biochem. 128*, 29−38.
22. Okada, K., Hirotsu, K., Hayashi, H., and Kagamiyama, H. (2001) *Biochemistry 40*, 7453−7463.
23. Kirsch, J. F., Eichele, G., Ford, G. C., Vincent, M. G., Jansonius, J. N., Gehring, H., and Christen, P. (1984) *J. Mol. Biol. 174*, 497−525.
24. Toney, M. D., and Kirsch, J. F. (1993) *Biochemistry 32*, 1471−1479.
25. Galburt, E., and Stoddard, B. L. (2001) *Phys. Today*, *54*, 33−39.
26. Otwinowski, Z., and Minor, W. (1996) *Methods Enzymol. 276*, 307−326.
27. Navaza, J. (1994) *Acta Crystallogr. A50*, 157−163.
28. CCP4 Collaborative Computational Project, Number 4 (1994) The CCP4 Suite: Programs for Protein Crystallography, *Acta Crystallogr. D50*, 760−763.
29. Brunger, A. T., Adams, P. D., Clore, G. M., DeLano, W. L., Gros, P., Grosse-Kunstleve, Jiang, J. S., Kuszewski, J., Nilges, M., Pannu, N. S., Read, R. J., Rice, L. M., Simonson, T., and Warren, G. L. (1998) *Acta Crystallogr. D54*, 905−921.
30. Jones, T. A., and Kjeldgaard, M. (1997) *Methods Enzymol. 277*, 173−208.
31. Kleywegt, G. J., and Jones, T. A. (1997) *Methods Enzymol. 277*, 208−230.
32. Kabsch W. (1976) LSQKAB, *Acta Crystallogr. A32*, 922−923.
33. Laskowski, R. A., MacArthur, M. W., Moss, D. S., and Thornton, J. M. (1993) *J. Appl. Crystallogr. 26*, 283−291.
34. Steiner, T., and Koellner, G. (2001) *J. Mol. Biol. 305*, 535−557.
35. Bondi, A. (1964) *J. Phys. Chem. 68*, 441−451.
36. Wood, Z. A., Poole, L. B., and Karplus, P. A. (2001) *Biochemistry 40*, 3900−3911.
37. Kerr, K. A., and Abraharns, J. P. (1975) *Acta Crystallogr. B31*, 2022−2026.
38. Gehring, H., and Christen, P. (1978) *J. Biol. Chem. 253*, 3158−3163.
39. Berezov, A., Iriarte A., and Martinez-Carrion M. (1994) *J. Biol. Chem. 269*, 22222−22229.
40. Schwede, T., Diemand A., Guex N., and Peitsch M. C. (2000) *Res. Microbiol. 151*, 107−112.
41. Lin, H. M., Kaneshige, M., Zhao, L., Zhang, X., Hanover, J. A., and Cheng, S. Y. (2001) *J. Biol. Chem. 276*, 48196−48205.
42. Than, N. G., Sumegi, B., Than, G. N., Bellyei, S., and Bohn, H. (2001) *Placenta 22*, 235−243.

BI020221C